Stable amplitude chimera in a network of coupled Stuart-Landau oscillators

K. Sathiyadevi,[1] V. K. Chandrasekar,[1,*] and D. V. Senthilkumar[2,†]
[1]*Centre for Nonlinear Science & Engineering, School of Electrical & Electronics Engineering, SASTRA Deemed University, Thanjavur-613 401, Tamil Nadu, India*
[2]*School of Physics, Indian Institute of Science Education and Research, Thiruvananthapuram-695016, India*

(Received 13 June 2018; revised manuscript received 17 August 2018; published 6 September 2018)

In many natural systems, attractive coupling together with repulsive coupling plays a vital role in determining their evolutionary dynamics. We investigate the stabilization of amplitude chimera through repulsive coupling in the presence of attractive coupling in a system of nonlocally coupled oscillators. The nonlocal repulsive coupling can facilitate the emergence of stable amplitude chimera even for random initial conditions contrasting with the earlier investigations, where the amplitude chimera was observed just as a transient state and that too for a specific cluster initial conditions. The stability of the observed amplitude chimera is analyzed using Floquet theory. To elucidate the transition among the distinct dynamical states, we find the average number of inhomogeneous oscillators as a function of the coupling strength and show that the transition among the dynamical states exhibits hysteresis. Further, we deduce analytically the critical stability curve that separates the oscillatory (amplitude chimera and traveling wave) states from the death (multi-incoherent oscillation death, cluster chimera death, cluster oscillation death) states. We also analyze the influence of the nonisochronicity parameter and noise on the stable amplitude chimera. We report that the nonisochronicity parameter favors the traveling wave state from incoherent death through the stable amplitude chimera state.

DOI: 10.1103/PhysRevE.98.032301

I. INTRODUCTION

The chimera state, an intriguing and counterintuitive collective dynamical behavior, has become an active area of research in recent years. It is characterized by the spontaneous splitting of a network of coupled identical oscillators into coexisting domains of coherent and incoherent dynamical states, as initially reported in nonlocally coupled phase oscillators by Kuramoto and Battogtokh [1–3]. Since then, a plethora of investigations have been carried out toward understanding the onset of chimera both theoretically and experimentally. Theoretical investigations have been carried out in coupled chaotic oscillators [4–6], neural networks [7,8], time discrete maps [9,10], planar oscillators [11], and so on. Recently, many complementary experimental observations have also been made to understand the robustness of such states in many natural and manmade systems. The first experimental observation was reported in optical systems [12] and chemical oscillators [13]. Later, chimera states were observed in mechanical oscillators [14,15], as well as electronic [16,17], electrochemical [18–20], optoelectronic delayed-feedback oscillators [21], Boolean networks [22], and optical combs [23]. Investigations of chimera states have revealed that such dynamical behavior bears a resemblance to the unihemispheric sleep of some mammals, migratory birds, and humans [24–26] , epileptic seizures [27], and power grid blackouts [28], and it even has potential applications in social networks [29] and neural activities [7,30].

Distinct types of chimera states, including globally clustered chimera [31], amplitude mediated chimera [32,33], and spiral wave chimera [3,34], have been reported in the literature. Among them, recently a special type of chimera state was reported by Zakharova *et al.* [35] in a network of nonlocally coupled oscillators with symmetry-breaking coupling. In this state, coherent and incoherent dynamical behaviors emerge with respect to the amplitude of the oscillators, termed amplitude chimera, despite the fact that the oscillators in the network exhibit periodic oscillations with the same frequency and correlated phases. In a later study, the same group of authors analyzed the stability of the amplitude chimera using the Floquet theory, and they reported that the observed amplitude chimera is just a transient state [36]. In this connection, time delay was found to enhance the lifetime of such transient amplitude chimera significantly [37]. Further, the lifetime was found to decrease with an increase in the noise intensity [38]. Recently, stable amplitude chimera was observed in locally coupled oscillators in the presence of the nonisochronicity parameter. It was also reported that the stable amplitude chimera loses its stability upon deviating a few oscillators from the cluster initial states [39]. The transition from spatiotemporal chaos to coherent oscillation death and chimera death through an amplitude chimera was reported recently in coupled chaotic oscillators [40]. Very recently, the tradeoff between attractive and repulsive coupling was found to induce the onset of distinct collective dynamics, which shows the swing of the synchronized state, chimera, chimera death, and oscillatory cluster state [41]. In the present study, we will investigate the role of repulsive coupling in stabilizing the amplitude chimera. Indeed, we show that such a state does exist due to repulsive interaction and is more stable even with random initial conditions.

*Corresponding author.
†Corresponding author.

In particular, we unravel the onset of stable amplitude chimera in a network of nonlocally coupled Stuart-Landau oscillators with combined attractive and repulsive interactions. To start with, we analyze the emerging behavior of the coupled Stuart-Landau oscillators using the cluster initial conditions as employed in the earlier studies. Further, we will show that the repulsive coupling facilitates the emergence of stable amplitude chimera even for random initial conditions. Furthermore, the stability of the amplitude chimera is corroborated using the Floquet theory. The dynamical transition takes place from the traveling wave state to incoherent death through the stable amplitude chimera state. To delineate the transition among the distinct dynamical states, we have analyzed the average number of inhomogeneous oscillators in the observed dynamical states. Further, the dynamical transition is also analyzed with respect to distinct coupling ranges and is found to be robust in a wide range of both attractive and repulsive coupling ranges exhibiting a bell-shaped function with a Gaussian fit. Furthermore, we deduce the probability of the observed dynamical behaviors as a function of the coupling strength to illustrate the emergence of multistability. We have also deduced analytically the critical stability curve that delineate the oscillatory (amplitude chimera and traveling wave) states from the death (multi-incoherent oscillation death, cluster chimera death, cluster oscillation death) states. The effect of the nonisochronicity parameter is also analyzed by introducing it. The nonisochronicity parameter is known to induce either desynchronization [42] or a death state [43]. In contrast, to our surprise we found that the nonisochronicity parameter facilitates the existence of the traveling wave via stable amplitude chimera from the incoherent death state. We will also unravel the effect of Gaussian white noise on the stability of the amplitude chimera. Finally, the robustness of the dynamical behaviors in larger networks is also elucidated.

The structure of the paper is as follows: In Sec. II, we introduce our model of nonlocally coupled Stuart-Landau oscillators with combined attractive and repulsive couplings. In Sec. III, we demonstrate the emergence of stable amplitude chimera for both the cluster initial conditions and random initial conditions. We discuss the global dynamical behavior and multistabilities in Sec. IV, and we describe detailed transitions among the dynamical states in Sec. V. The analytical stability condition delineating the oscillatory and death states will be deduced in Sec. VI. Further, the effects of nonisochronicity parameter and the Gaussian white noise are investigated in Sec. VII. Finally, we summarize our results in Sec. VIII. The effect of the size of the network on the stable amplitude chimera is discussed in Appendix.

II. MODEL

The Stuart-Landau oscillator is a simple, paradigmatic model exhibiting limit cycle oscillations [44,45]. It is the normal form of the Hopf bifurcation, and hence many nonlinear oscillators exhibiting Hopf bifurcation can be approximated as the Stuart-Landau oscillator. Further, limit cycle oscillations can be seen often in biological and chemical systems, for example in circadian rhythms, bursting of neurons, and so on. Thus the Stuart-Landau limit cycle oscillators have been used widely to understand various collective dynamical states of nonlinear dynamical systems [46–48]. To elucidate the emergence of stable amplitude chimera, we consider a ring of nonlocally coupled Stuart-Landau oscillators with combined attractive and repulsive couplings, whose governing equations are represented as

$$\dot{z}_i = (\lambda + i\omega - |z_i|^2)z_i + \frac{\epsilon}{2P_1}\sum_{k=i-P_1}^{i+P_1} \mathrm{Re}(z_k - z_i) - i\frac{\epsilon}{2P_2}\sum_{k=i-P_2}^{i+P_2} \mathrm{Im}(z_k - z_i), \quad (1)$$

where the state variables $z_i = x_i + iy_i \in C$, $i = 1, 2, \ldots, N$, N is the total number of oscillators in the network. Here, λ and ω correspond to the bifurcation parameter and the natural frequency of the system, respectively. The attractive coupling is established through the state variables x_i whereas the repulsive coupling is accomplished via y_i variables [49]. ϵ is the strength of the attractive and repulsive couplings. P_1 and P_2 represent the number of nearest neighbors in the attractive and repulsive couplings, respectively, with the corresponding coupling ranges r_1 ($r_1 = P_1/N$) and r_2 ($r_2 = P_2/N$). The Runge-Kutta fourth-order integration scheme is used for all our simulations with time step 0.01.

III. STABLE AMPLITUDE CHIMERA

To unravel the influence of the repulsive interaction on the reported transient amplitude chimera, we have fixed the parameters at $r_1 = 0.01$, $\omega = 2.0$, and $\lambda = 1.0$ of the attractive coupling as in the earlier studies [39]. It is evident from the earlier reports that the amplitude chimera exist for a specific choice of cluster initial conditions, which can be obtained by dividing the network of oscillators into two parts and distributing the initial states $(x_i, y_i) = (+1, -1)$ for $i = 1, 2, \ldots, N/2$ and $(x_i, y_i) = (-1, +1)$ for $i = \frac{N}{2} + 1, \ldots, N$. To start with, the emergence of stable amplitude chimera in the coupled Stuart-Landau oscillators will be elucidated by distributing the above-mentioned cluster initial conditions. We have fixed the total number of oscillators in the network as $N = 100$ in the entire manuscript. The effect of an increase in the size of the network on the observed dynamical transitions will be discussed in Appendix. The transient behavior for the coupling strength $\epsilon = 2.02$ is shown in the space-time plot of Fig. 1(a), which depicts that the oscillators at the cluster edges attain inhomogeneous states spontaneously and oscillate incoherently as time increases. The phase portrait of the corresponding state after leaving 5×10^3 time units as transient is shown in Fig. 1(c). The solid (gray) and dashed lines (pink and blue) correspond to the phase portrait of the homogeneous and inhomogeneous oscillations, respectively. It is evident from the phase portrait that the coherent oscillators oscillate about the origin with a large amplitude, whereas the incoherent oscillators oscillate with relatively smaller amplitudes constituting the upper and lower branches of the inhomogeneous state. The observed dynamical behavior is also examined for its emergence by distributing random initial conditions among the oscillators. Surprisingly, we found that the stable amplitude chimera emerges even for random initial conditions in contrast to the earlier observations of it using only the cluster initial

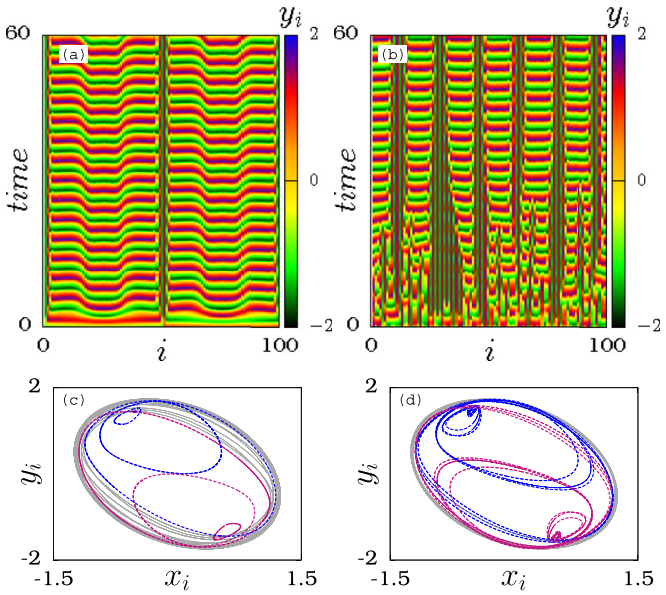

FIG. 1. The space-time plot and phase portrait of stable amplitude chimera at $\epsilon = 2.02$ for (a) cluster initial conditions and (b) random initial conditions. In (c) and (d) the solid and dotted lines correspond to the homogeneous and inhomogeneous oscillations, respectively. Other parameters: $r_1 = 0.01$, $r_2 = 0.22$, $\omega = 2.0$, $\lambda = 1.0$, and $N = 100$.

conditions. The amplitude chimera emerging from the random initial condition is depicted in Figs. 1(b) and 1(d). From Fig. 1(b), it is evident that all the oscillators initially oscillate randomly, attributed to the random initial conditions, which eventually split into coherent and incoherent domains as they evolve. The corresponding phase portrait is shown in Fig. 1(d). The observed amplitude chimera is stable and all the oscillators oscillate periodically with the same frequency. The emergence of (stable/unstable) amplitude chimera has been reported so far in the literature only for cluster initial conditions. In contrast, we have unraveled the existence of stable amplitude chimera even for random initial states, as is evident from Fig. 1(b).

Now, we use the Floquet theory to substantiate whether the observed amplitude chimera is a long transient or a stable state. For this purpose, we substitute $x_i = x_i^* + \eta_i$ and $y_i = y_i^* + \zeta_i$ in Eq. (1), so that the system of Eq. (1) can be reduced as

$$\dot{\eta}_i = q_1\eta_i - (\omega + 2x_i^* y_i^*)\zeta_i + \frac{\epsilon}{2P_1}\sum_{k=i-P_1}^{i+P_1}(\eta_k - \eta_i),$$

$$\dot{\zeta}_i = (\omega - 2x_i^* y_i^*)\eta_i + q_2\zeta_i - \frac{\epsilon}{2P_2}\sum_{k=i-P_2}^{i+P_2}(\zeta_k - \zeta_i), \quad (2)$$

where $q_1 = 1 - 3x_i^{*2} - y_i^{*2}$, $q_2 = 1 - x_i^{*2} - 3y_i^{*2}$. Here x_i^* and y_i^* are the solutions of the amplitude chimera (AC), and η_i and ζ_i are their perturbation terms. The corresponding Floquet multipliers are found from the fundamental matrix by integrating Eq. (2) for one period [36]. Whenever the value of the Floquet multipliers is less than unity, then the corresponding periodic orbit is stable. Usually one of the eigenvalues is always designated by the unit value, which is referred to as the Goldstone mode in the literature. To elucidate the stability of the periodic orbit, the values of the Floquet multipliers are depicted in Fig. 2. Lines connecting open circles (blue) and triangles (red) correspond to the values of the Floquet multipliers for random and cluster initial conditions, respectively. It is evident from Fig. 2 that the value of all $|\mu_j|$ are less than unity except $|\mu_1|$ (Goldstone mode), which corroborate that the periodic orbits constituting the amplitude chimera are stable.

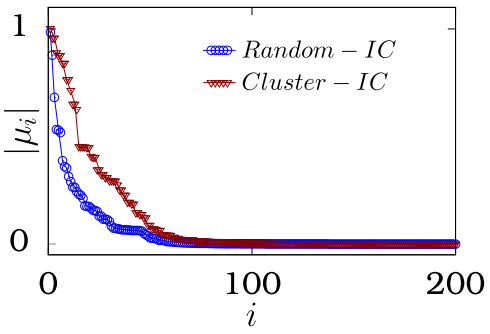

FIG. 2. Floquet multipliers $|\mu_i|$ for the stable amplitude chimera state at $\epsilon = 2.02$, $i = 1, 2, \ldots, 2N$ ($N = 100$). The unfilled circles connected by a line represent $|\mu_i|$ for random initial conditions, and unfilled triangles with a line denote $|\mu_i|$ for cluster initial conditions.

Further, there is a transition to stable amplitude chimera state from the traveling wave state and finally to the multi-incoherent death state as a function the coupling strength ϵ. The observed dynamical transition is depicted as space-time plots in Figs. 3(a)–3(c). For the coupling strength $\epsilon = 1.9$, the system (1) exhibits a traveling wave [see Fig. 3(a)],

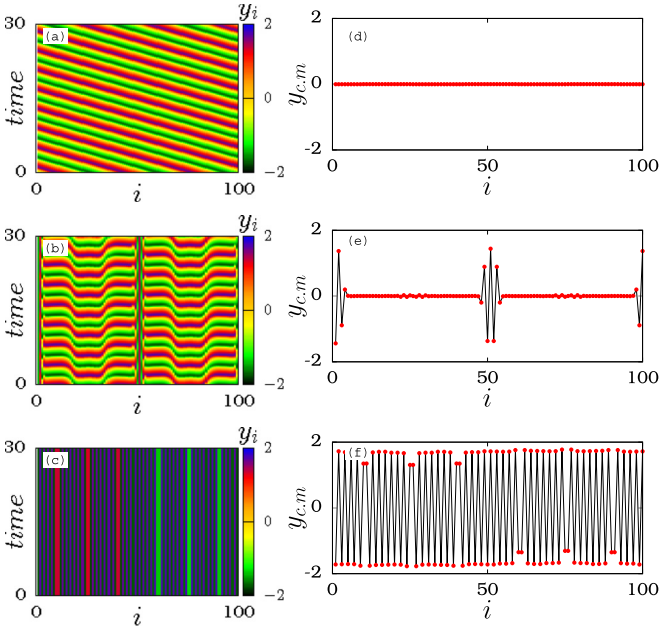

FIG. 3. The space-time plots of the variable y_i: (a) Traveling-wave state for $\epsilon = 1.9$, (b) amplitude chimera for $\epsilon = 2.02$, (c) multi-incoherent death state for $\epsilon = 2.6$; (d) and (e) correspond to the center of mass of the left panel (a)–(c), respectively. Other parameter values are the same as in Fig. 1.

where the oscillators in the network oscillate with the same amplitude and frequency, traveling with constant velocity. Upon increasing the coupling strength to $\epsilon = 2.02$, the coherent part oscillates with the same amplitude while the incoherent part suffers variations in their amplitude [see Fig. 3(b)]. Increasing the coupling strength further to $\epsilon = 2.6$ leads to multi-incoherent oscillation death [see Fig. 3(c)]. In this state, the oscillators in the network populate the upper and the lower branch of different inhomogeneous steady states alternately. To distinguish the dynamical states and to differentiate the domains of homogeneous and inhomogeneous oscillations, we have calculated the center of mass using the formula $y_{i_{\text{c.m.}}} = \int_0^T \frac{y_i(t)dt}{T}$, where $T = \frac{2\pi}{\omega}$ is the period of oscillation [35]. From Fig. 3(d), it is clear that all the oscillators oscillate homogeneously about the origin in the traveling wave (TW) state, whereas some of the oscillators take the nonzero center of mass contributing to the inhomogeneous states of the stable amplitude chimera in Fig. 3(e). The nonzero center of mass of all the oscillators in the multi-incoherent death state in Fig. 3(f) indicates that all the oscillators populate inhomogeneous states. The global dynamical behavior as a function of the repulsive nonlocal coupling range is illustrated in the following section.

IV. GLOBAL BEHAVIOR AND MULTISTABLE NATURE

To understand the global dynamical behavior, we have depicted the two-parameter bifurcation diagram in the (r_2, ϵ) space in Fig. 4. It is evident from the figure that the traveling wave state prevails in the entire range of r_2 for lower values of the coupling strength ϵ. Transition from the TW to multi-incoherent oscillation death (MIOD) via stable amplitude chimera (AC) is observed as a function of ϵ in the entire range of r_2. Further, the spread of stable AC is more pronounced around $r_2 = 0.25$. It is also clear that multistability among the distinct states can be observed between the boundary of the traveling wave and the amplitude chimera. Regions R_1 and R_3 indicate the bistability between TW-AC and AC-MIOD, respectively. Tristability is found in the region R_2 where the coexistence of all three states TW, AC, and MIOD prevails.

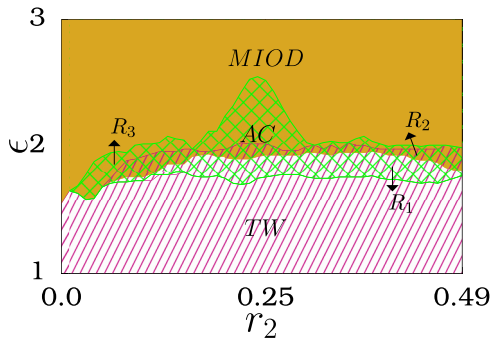

FIG. 4. Two-parameter bifurcation diagram in (r_2, ϵ) space for 100 realizations of distinct initial conditions. TW, AC, and MIOD represent the traveling wave, amplitude chimera, and multi-incoherent oscillation death state, respectively. R_1, R_2, and R_3 denote the multistability regions of TW-AC, TW-AC-MIOD, and AC-MIOD, respectively. Other parameters: $r_1 = 0.01$, $\lambda = 1.0$, $\omega = 2.0$, and $N = 100$.

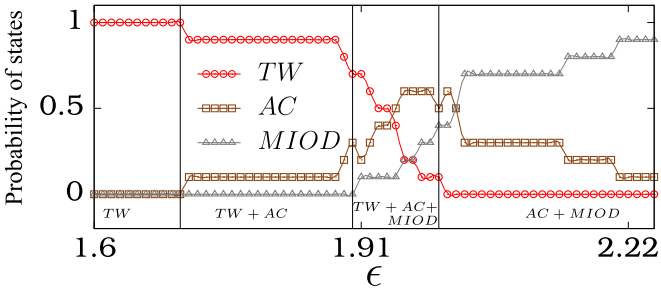

FIG. 5. Probability of occurrence of TW, AC, and MIOD states with respect to the coupling strength ϵ for 100 realization of distinct cluster and random initial conditions. Other parameters: $r_1 = 0.01$, $r_2 = 0.22$, $\omega = 2.0$, $\lambda = 1.0$, and $N = 100$.

Using the probability of the observed dynamical states, the multistable nature of the considered system is elucidated in Fig. 5. We have calculated the maximum probability of the occurrence of the observed dynamical states in Fig. 5 as we have made 100 realizations using the cluster initial conditions and 100 realizations using the random initial conditions to estimate the probability of the states. Essentially, one may observe all the states depicted in Fig. 5 either for cluster initial conditions or for random initial conditions, but their probabilities may vary depending on the specific initial conditions that are being used.

The unstable nature of a dynamical state can be revealed by the null value of the probability of the corresponding state. The probability of the states between zero and unity indicates the multistable nature of the dynamical states. The unit value of the probability of a state corroborates its monostable nature. It is clear from Fig. 5 that initially the system exhibits a monostable state with the traveling wave state as the only stable state with its probability acquiring unit value. While increasing the coupling strength, the system attains bistability, where the probabilities of AC and TW take nonzero values that are less than unity. The probability of the incoherent death state acquires null value in the bistability region. Upon increasing ϵ, the coupled Stuart-Landau oscillators exhibit tristability between TW, AC, and MIOD states. At large coupling limits, the probability of these states illustrates that the system again attains a monostable state via bistability. Transitions among the observed dynamical states are delineated more clearly in the following section.

V. DYNAMICAL TRANSITIONS

In general, a multistable system has the tendency to exhibit hysteresis during the dynamical transition between different states [50]. To unravel the existence of hysteresis among the observed dynamical states, we introduce a new statistical measure for finding the average number of inhomogeneous oscillators in a dynamical state using the relation

$$K = 1 - \frac{\sum_{i=1}^{N} H_{y_i}}{N}, \quad H_{y_i} = \Theta(\delta - y_{i_{\text{c.m.}}}). \tag{3}$$

Here δ is a predefined threshold value and $\Theta(\cdot)$ is the Heaviside step function. $y_{i_{\text{c.m.}}}$ is the center of mass of each of the oscillators. The average number of inhomogeneous

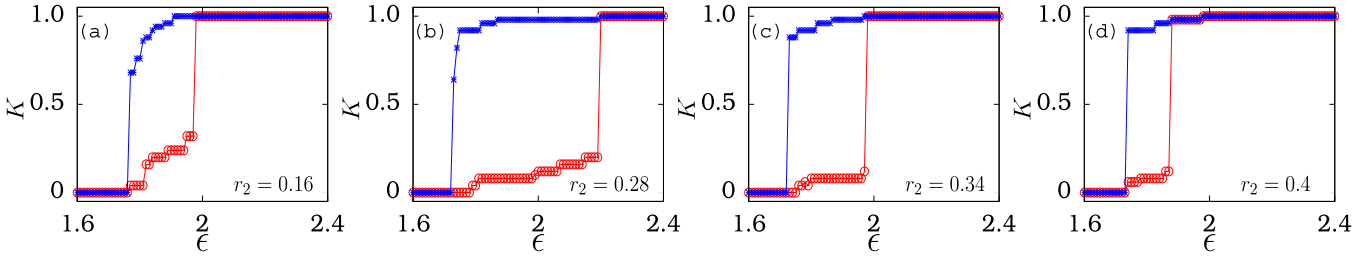

FIG. 6. The average number of oscillators in the inhomogeneous state (K) as a function of the coupling strength ϵ for the coupling range (a) $r_2 = 0.16$, (b) $r_2 = 0.28$, (c) $r_2 = 0.34$, and (d) $r_2 = 0.40$. Lines connected by open circles (blue) and stars (red) represent forward and reverse transitions, respectively. Other parameters: $r_1 = 0.01$, $\lambda = 1.0$, $\omega = 2.0$, and $N = 100$.

oscillators (K) acquires null value for the traveling wave state and unity for the incoherent death state. The value of K between $0 < K < 1$ corroborates the amplitude chimera. To understand the nature of the transition among the observed dynamical states, we have plotted the average number of oscillators in the inhomogeneous state (K) as a function of the coupling strength ϵ for distinct coupling ranges (see Fig. 6). Open circles and stars in Fig. 6 denote forward and reverse traces of the dynamical transition, respectively. The transition among the dynamical states is plotted for a lower repulsive coupling range $r_2 = 0.16$ in Fig. 6(a). Increasing the coupling strength, we found that there is a continuous transition from the traveling wave state to the stable AC state. The dynamical states during the forward and reverse traces are depicted as space-time plots in panel (A) and panel (B), respectively, of Fig. 7 for different ε. The coupled system exhibits a traveling wave state, which is completely characterized by homogeneous oscillations, as depicted in Fig. 7(a) for $\varepsilon = 1.76$. Upon increasing the coupling strength to $\varepsilon = 1.77$, the system exhibits amplitude chimera as shown in Fig. 7(b), whose dynamical states are characterized by homogeneous oscillations along with a few inhomogeneous oscillatory states [see Figs. 1(c) and 1(d) for homogeneous and inhomogeneous oscillatory states]. A further increase in ε results in stable amplitude chimera with a large number of inhomogeneous oscillatory states as depicted in Figs. 7(c) and 7(d) for $\varepsilon = 1.85$ and 1.9, respectively. At $\varepsilon = 1.98$, there is a sudden transition from amplitude chimera to the MIOD state, which is completely characterized by an inhomogeneous oscillation death state, thereby elucidating the first-order (discontinuous) transition [see Fig. 6(a)]. The MIOD state exhibited by the system for $\varepsilon = 2.0$ is shown in Fig. 7(e).

On the other hand, during the reverse trace by decreasing ε, there is a continuous transition from the MIOD state to amplitude chimera and a discontinuous (first-order) transition from amplitude chimera to a traveling wave state as depicted in Fig. 6(a). Thus the array of coupled Stuart-Landau oscillators exhibits hysteresis as a function of the coupling strength ε. During the backward trace, the MIOD state [see Fig. 7(a) for $\varepsilon = 2.0$ in panel B] is completely characterized by inhomogeneous oscillation death. Upon decreasing the value of ε, the amplitude chimera is characterized by inhomogeneous oscillations with a very few homogeneous oscillatory states as in Fig. 7(b) of panel B for $\varepsilon = 1.9$. A further decrease in ε leads to the amplitude chimera with a large number of homogeneous oscillatory states as in Figs. 7(c) and 7(d) of panel B for $\varepsilon = 1.85$ and 1.77, respectively. At $\varepsilon = 1.76$, there is a sudden (discontinuous) transition to a traveling wave state [see Fig. 7(e) in panel B], which is completely characterized by a homogeneous oscillatory state. We have also noticed that the system exhibits a similar dynamical transition for further increase in the coupling range with variations in the hysteresis width. It increases up to the coupling range $r_2 = 0.24$, which is further decreased by increasing the coupling range

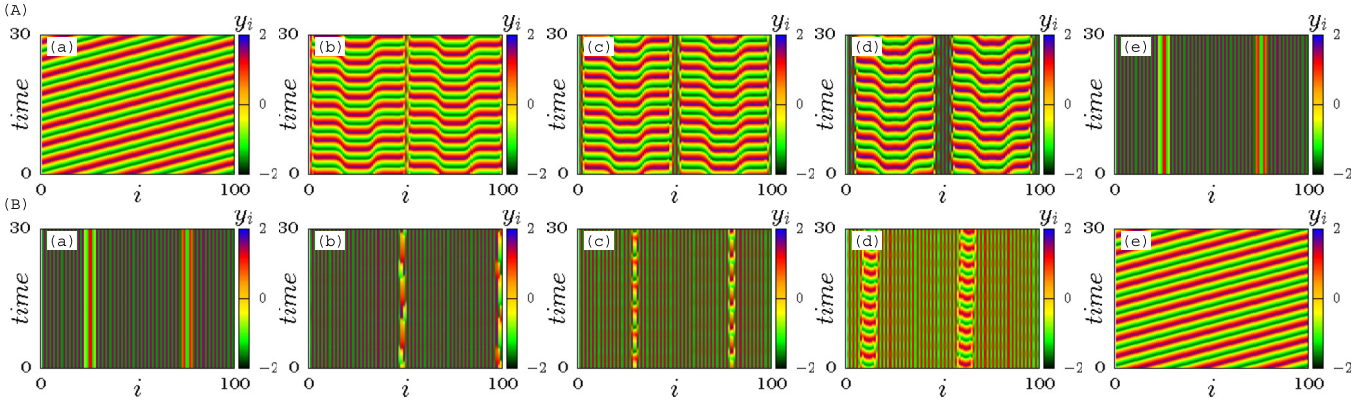

FIG. 7. Space-time plots of a dynamical transition along forward [panel (A)] and reverse [panel (B)] transition for $r_2 = 0.16$. Panel (A): (a) traveling wave state for $\epsilon = 1.76$; (b)–(d) amplitude chimera state for $\epsilon = 1.77$, $\epsilon = 1.85$, and $\epsilon = 1.9$; (e) multi-incoherent oscillation death for $\epsilon = 2.0$. Panel (B): (a) multi-incoherent oscillation death for $\epsilon = 2.0$; (b)–(d) amplitude chimera state for $\epsilon = 1.9$, $\epsilon = 1.85$, and $\epsilon = 1.77$; (e) traveling wave state for $\epsilon = 1.76$.

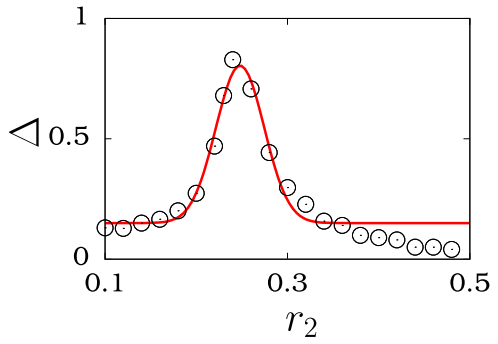

FIG. 8. The width of the hysteresis as a function of the nonlocal coupling range r_2. The unfilled circles (black) denote the numerical data.

[see Figs. 6(b), 6(c), and 6(d) for $r_2 = 0.28$, $r_2 = 0.34$, and $r_2 = 0.4$, respectively].

We have also estimated the variation in the width of the hysteresis with respect to the repulsive coupling range r_2 (see Fig. 8). By increasing the coupling range, the width of the hysteresis is found to increase up to $r_2 = 0.24$ and attains the maximum value at $r_2 = 0.24$. A further increase in the coupling range leads to a decrease in the width of the hysteresis to a minimum value. Thus the width of the hysteresis forms a bell-shaped function and it obeys a Gaussian fit as a function of the nonlocal repulsive coupling.

To understand the dynamical transition at higher values of nonlocal attractive coupling ranges, we have plotted a space-time pattern and snapshot for the coupling ranges $r_1 = 0.4$ and $r_2 = 0.34$ in Fig. 9. The transition to chimera death was observed through AC and cluster oscillation death (COD) while increasing the coupling strength ϵ. The amplitude chimera was observed at $\epsilon = 1.7$ [see Figs. 9(a) and 9(b)] with four groups of coherent and incoherent patches. For smaller values of attractive coupling (up to $r_1 = 0.07$), the coherent domain of the amplitude chimera is composed of symmetric attractors with zero center of mass as shown in Figs. 3(b) and 3(e). On the other hand, for higher values of r_1 the coherent domains of the amplitude chimera are characterized by asymmetric attractors with nonzero center of mass as depicted in Figs. 9(a) and 9(b). By increasing the coupling strength to $\epsilon = 2.0$, all the oscillators populate the inhomogeneous steady state resulting in a coherent COD state [see Figs. 9(c) and 9(d)]. Increasing ϵ to much higher values leads to chimera death where the oscillators in the clusters edges populate the upper and lower branches of the inhomogeneous steady state as shown in Figs. 9(e) and 9(f) for $\epsilon = 2.3$. Further, to delineate the global dynamical behavior for higher values of nonlocal attractive coupling, we have plotted the two-parameter bifurcation diagram in the (r_2, ϵ) space for two distinct values of the attractive coupling, $r_1 = 0.2$ and $r_1 = 0.4$, in Fig. 10. We have found COD and cluster chimera death (CCD) from the amplitude chimera state instead of the MIOD state (see Fig. 4) because of the influence of much stronger nonlocal attractive coupling. The coexistence of COD and CCD states is observed at strong coupling strengths depending on the initial conditions. Moreover, the number of clusters in the observed COD and CCD states decreases exponentially upon

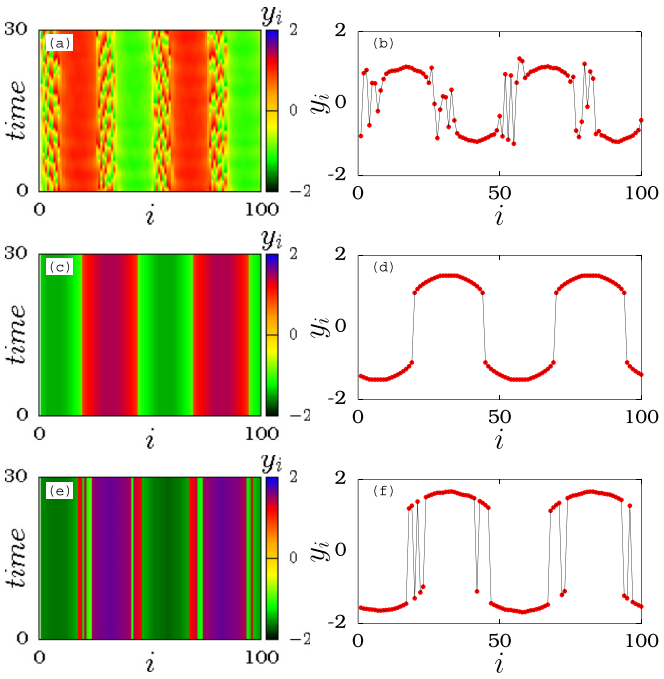

FIG. 9. The space-time plots and snapshots of the variables y_i as a function of coupling strength ϵ displaying (a),(b) amplitude chimera for $\epsilon = 1.7$, (c),(d) cluster oscillation death (COD) for $\epsilon = 2.0$, and (e),(f) cluster chimera death (CCD) for $\epsilon = 2.3$. Other parameters: $r_1 = 0.4$, $r_2 = 0.34$, $\lambda = 1.0$, $\omega = 2.0$, and $N = 100$.

increasing the coupling range r_2 as shown in Figs. 10(c) and 10(d). The corresponding log-log plot is depicted in the inset of Figs. 10(c) and 10(d), which clearly elucidates that the number of clusters in the observed COD and CCD states obeys power-law $n_0 = a * (r_2)^b$ as a function of r_2 [51], where b takes the values -0.613 and -0.569, respectively. The

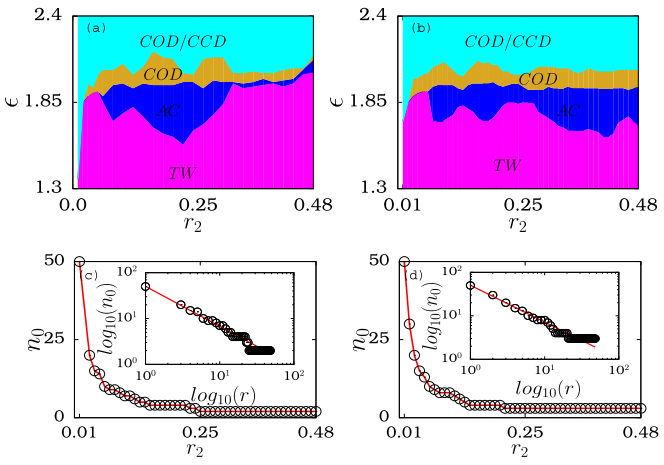

FIG. 10. Two-parameter diagrams in (r_2, ϵ) space, for the coupling ranges (a) $r_1 = 0.2$ and (b) $r_1 = 0.4$. Parts (c) and (d) show an exponential decrease of cluster size for $r_1 = 0.2$ and $r_1 = 0.4$ as a function of the coupling range r_2 for $\epsilon = 1.98$. The corresponding power-law fit is shown in the inset in logarithmic scale. Unfilled circles represent the numerical data, and the corresponding best fit is shown by a red solid line.

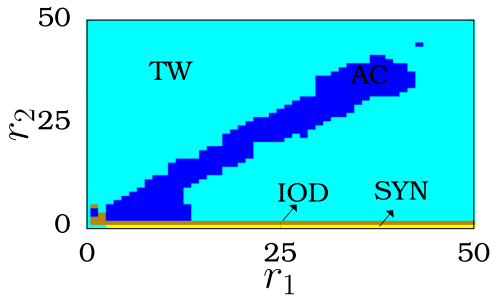

FIG. 11. Two-parameter phase diagram in (r_1, r_2) space for $\epsilon = 1.7$. TW, AC, IOD, and SYN denote the traveling wave, amplitude chimera, incoherent oscillation death, and synchronized state, respectively. Other parameters are the same as in Fig. 9.

unfilled circles correspond to the numerical data along with the fitting denoted by solid line in Figs. 10(c) and 10(d).

The observed dynamical transitions are delineated in the two-phase diagram (see Fig. 11) as a function of r_1 and r_2 to corroborate the robustness of the unraveled dynamical states in the coupled Stuart-Landau oscillators. The coupling strength is fixed as $\varepsilon = 1.7$, while the values of the other parameters are the same as in Fig. 9. The coupled system exhibits only the traveling wave state as a function of the repulsive coupling range for $r_1 = 0$. On the other hand, the coupled system exhibits only the synchronized state as a function of the attractive coupling range in the absence of the repulsive coupling. Interesting nonlinear dynamical behaviors and their transitions are observed in the presence of both the attractive and repulsive couplings. In particular, the stable amplitude chimera is observed in a wide range of both r_1 and r_2 as evident from Fig. 11. Further, the IOD state (a constituent of MIOD state) is also found as a function of the attractive coupling range for smaller values of the repulsive coupling range. It should be noted that the IOD state always coexists with the death states (MIOD, COD, CCD).

VI. STABILITY CONDITION FOR THE INCOHERENT OSCILLATION DEATH STATE

Deducing exact solutions corresponding to the observed dynamical states is extremely difficult and often impossible. However, there always lies a boundary between the oscillatory states and the death states (see Figs. 4, 10, and 14). By finding the stability condition for the death (IOD) state, one can obtain an analytical critical curve that serves as the boundary between the oscillatory and the death states. Here, we deduce the stability condition corresponding to the critical curve above which the IOD state, where the oscillators in the network populate the upper and lower branches of the inhomogeneous steady state alternately [see Fig. 3(f)], is stable. In this state, the system has the solutions $(x_i, y_i) = (x, y)$ if i is odd and $(x_i, y_i) = (-x, -y)$ if i is even or vice versa. On substituting the above solutions, to obtain the analytical condition for the critical (stability) curve, the system (1) can be reduced as

$$\begin{aligned}\dot{x} &= (\lambda - x^2 - y^2)x - \omega y - \beta_1 x,\\ \dot{y} &= (\lambda - x^2 - y^2)y + \omega x + \beta_2 y,\end{aligned} \tag{4}$$

TABLE I. The values of β_1 and β_2 with respect to P_1 and P_2.

P_1	P_2	β_1	β_2
even	even	ϵ	ϵ
even	odd	ϵ	$\left(\frac{P_2+1}{P_2}\right)\epsilon$
odd	even	$\left(\frac{P_1+1}{P_1}\right)\epsilon$	ϵ
odd	odd	$\left(\frac{P_1+1}{P_1}\right)\epsilon$	$\left(\frac{P_2+1}{P_2}\right)\epsilon$

where β_1 and β_2 are defined based on the odd and even numbers of the nearest neighbor listed in Table I.

Now, the solution for the dynamical Eq. (4) can be deduced as

$$\begin{aligned}x(t) &= \frac{e^{\frac{1}{2}\gamma_1 t}\cos\left(\delta - \frac{1}{2}\psi_1 t\right)}{\left(C - \frac{1}{4}e^{\gamma_1 t}[V_0 + V_1\cos(\psi_1 t) + V_2\sin(\psi_1 t)]\right)},\\ y(t) &= \frac{1}{\omega}\left(\frac{-\hat{\beta}}{2} + \psi_1\tan(\psi_1 t - \delta)\right)x(t),\end{aligned} \tag{5}$$

where $\psi_1 = \sqrt{4\omega^2 - \hat{\beta}^2}$, $\hat{\beta} = \beta_1 + \beta_2$, $\gamma_1 = \beta_2 - \beta_1 + 2\lambda$, and C and δ are integration constants. The other constants V_0, V_1, and V_2 are

$$\begin{aligned}V_0 &= \frac{-8}{\gamma_1}, \quad V_1 = \frac{\hat{\beta}[k_1\cos(2\delta) + k_2\sin(2\delta)]}{k_3},\\ V_2 &= \frac{\hat{\beta}[-k_2\cos(2\delta) + k_1\sin(2\delta)]}{k_3},\end{aligned} \tag{6}$$

where $k_1 = \beta_1^2 + \beta_1(\beta_2 - \lambda) - \beta_2\lambda - 2\omega^2$, $k_2 = (\beta_1 - \lambda)\psi_1$, and $k_3 = \omega^2[(\lambda - \beta_1)(\lambda + \beta_2)] + \omega^2$. The solution (5) is found to be periodic when $\omega > \frac{\hat{\beta}}{2}$. In this case, we can write the state variables $x(t)$ and $y(t)$ in the asymptotic limit as

$$\begin{aligned}x(t) &= \frac{\cos\left(\delta - \frac{1}{2}\psi_1 t\right)}{[V_0 + V_1\cos(\psi_1 t) + V_2\sin(\psi_1 t)]^{\frac{1}{2}}},\\ y(t) &= \frac{-1}{\omega}\frac{\left(\frac{\hat{\beta}}{2}\cos(\delta - \frac{1}{2}\psi_1 t) - \psi_1\sin(\delta - \frac{1}{2}\psi_1 t)\right)}{[V_0 + V_1\cos(\psi_1 t) + V_2\sin(\psi_1 t)]^{\frac{1}{2}}}.\end{aligned} \tag{7}$$

On the other hand, the solution (5) turns out to be a decaying solution for $\omega < \frac{\hat{\beta}}{2}$, which can be deduced as

$$\begin{aligned}x(t) &= \frac{e^{\frac{1}{2}\gamma_1 t}\cos\left(\delta - \frac{1}{2}\theta_1 t\right)}{\left(C - \frac{1}{2\omega^2}e^{\gamma_1 t}[W_0 + W_1\cos(\theta_1 t) + W_2\sin(\theta_1 t)]\right)^{\frac{1}{2}}},\\ y(t) &= \frac{1}{\omega}\left(\frac{-\hat{\beta}}{2} + \theta_1\tan(\theta_1 t - \delta)\right)x(t),\end{aligned} \tag{8}$$

where $\theta_1 = \sqrt{\hat{\beta}^2 - 4\omega^2}$. The other constants W_0, W_1, and W_2 are

$$\begin{aligned}W_0 &= \frac{\hat{\beta}^2}{\gamma_1}, \quad W_1 = \frac{\hat{\beta}[l_1\cos(2\delta) + l_2\sin(2\delta)]}{l_3},\\ W_2 &= \frac{\hat{\beta}[-l_2\cos(2\delta) + l_1\sin(2\delta)]}{l_3},\end{aligned} \tag{9}$$

where $l_1 = (\beta_1 + \beta_2)^3 + 8(\lambda - \beta_1)\omega^2$, $l_2 = (-\beta_1^2 + \beta_2^2 + 2\lambda\hat{\beta} - 4\omega^2)$, and $l_3 = -\beta_1^2 + \beta_2^2 - 2\lambda(\beta_2 - \beta_1) + 2(\lambda^2 -$

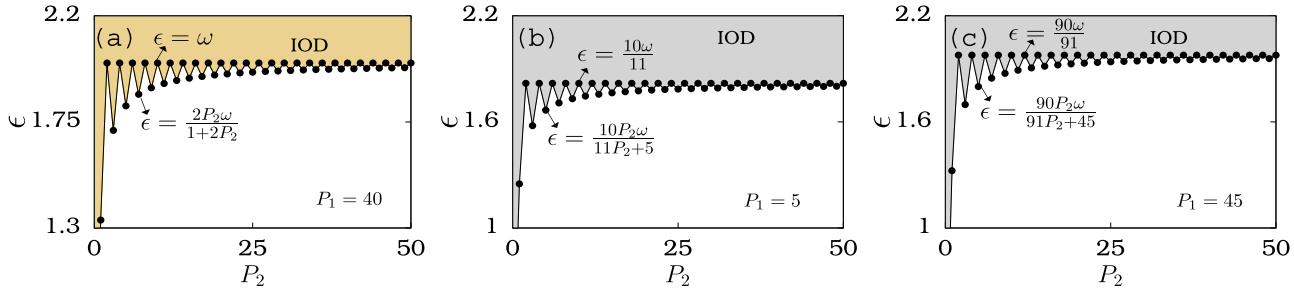

FIG. 12. Stability curves of IOD regions for even and odd values of P_1 ($r_1 = \frac{P_1}{N}$) as a function of P_2 ($r_2 = \frac{P_2}{N}$). (a) $P_1 = 40$, (b) $P_1 = 5$, and (c) $P_1 = 45$. The shaded region corresponds to the numerically obtained IOD region.

ω^2). In the asymptotic limit, $x(t)$ and $y(t)$ approach constant values leading to a pair of steady states given by

$$x^* = \mp\frac{1}{\sqrt{2}}\sqrt{\frac{\tilde{\lambda}(\hat{\beta} - \sqrt{\hat{\beta}^2 - 4\omega^2}) + 2\omega^2}{\hat{\beta}}},$$
$$y^* = \pm\frac{\hat{\beta} + \sqrt{\hat{\beta}^2 - 4\omega^2}}{2\omega}x^*, \tag{10}$$

where $\tilde{\lambda} = \lambda - \beta_1$ and $\hat{\beta} = \beta_1 + \beta_2$. Carrying out the linear stability analysis of Eq. (1) around the deduced steady states $(\pm x^*, \pm y^*)$, depending on even or odd values of i, one can obtain the stability conditions for the IOD state. The stability conditions depend on the distinct pairs of odd and even values of the nearest neighbor in the nonlocal coupling listed in Table II. The stable region of the IOD state emerges for $\epsilon \geqslant \omega$ when P_2 is even and $\epsilon \geqslant \frac{2p_2\omega}{1+2P_2}$ when P_2 is odd. The stability curve for an even value of P_1 ($P_1 = 40$) is shown in Fig. 12(a) as a function of P_2. The stability curve is the same for all even values of P_1 as the stability condition is independent of P_1. For odd P_1, P_2 may be even or odd. The stable region of the IOD state emerges for $\epsilon \geqslant \frac{2p_1\omega}{1+2P_1}$ when P_2 is even and $\epsilon \geqslant \frac{2P_1P_2\omega}{P_1+P_2+2P_1P_2}$ when P_2 is odd. The stability curves for odd values of P_1 are shown in Figs. 12(b) and 12(c) for $P_1 = 5$ and 45, respectively. Thus the death states are stable above the stability curve, while the oscillatory states are stable below the critical curve. The oscillatory states can be amplitude chimera or a traveling wave depending on the initial conditions and the parameters involved. Similarly, the death states can be MIOD, COD, or CCD, again depending on the initial conditions and the parameters. The shaded and the unshaded regions in Fig. 12 correspond to the numerically obtained IOD region and the oscillatory region, respectively, corroborating the exact coincidence of a numerical boundary between them and the critical stability curve deduced analytically.

TABLE II. Stability condition with respect to P_1 and P_2.

Stability conditions for IOD state		
P_1	P_2	condition
even	even	$\epsilon \geqslant \omega$
even	odd	$\epsilon \geqslant \frac{2p_2\omega}{1+2P_2}$
odd	even	$\epsilon \geqslant \frac{2p_1\omega}{1+2P_1}$
odd	odd	$\epsilon \geqslant \frac{2P_1P_2\omega}{P_1+P_2+2P_1P_2}$

VII. EFFECT OF THE NONISOCHRONICITY PARAMETER AND NOISE INTENSITY

Nonisochronicity-induced stable amplitude chimera was reported recently by Premalatha *et al.* in a locally coupled Stuart-Landau oscillator [39]. Now, we investigate the effect of the nonisochronicity parameter on the stable amplitude chimera. The dynamical behavior of the system in the presence of the nonisochronicity parameter is shown as space-time plots and the center of mass of the dynamical variables y_i in Fig. 13 for the nonlocal coupling strength $\epsilon = 2.7$. Initially, the system exhibits a multi-incoherent death state for lower values of the nonisochronicity parameter as shown in Figs. 13(a) and 13(b) for $c = 0.1$. By increasing the nonisochronicity parameter, the emergence of stable amplitude chimera is observed at $c = 0.5$ [see Figs. 13(c) and 13(d)]. Upon increasing the nonisochronicity parameter further to $c = 0.8$, the system exhibits a coherent traveling wave state, which is depicted in Figs. 13(e) and 13(f). Interestingly, in

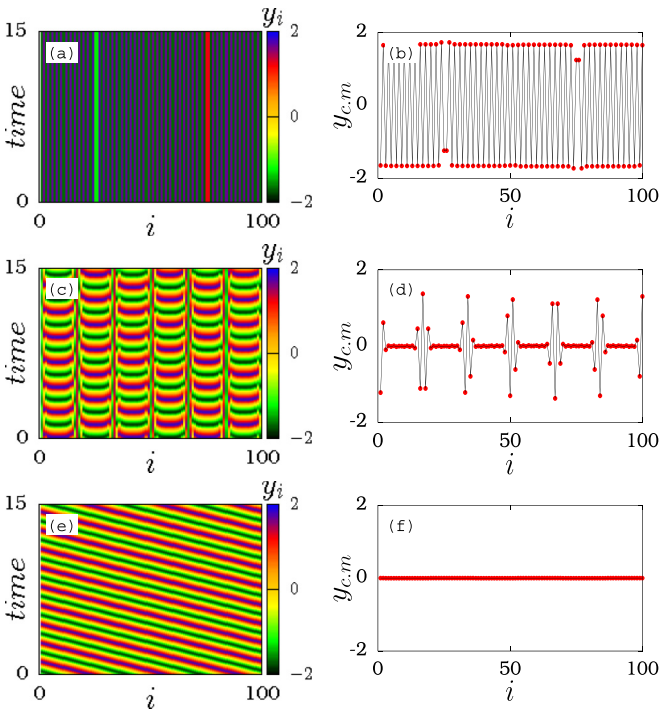

FIG. 13. The space-time plots and time average of the variable y_i of each of the oscillators: (a),(b) MIOD for $c = 0.1$, (c),(d) AC for $c = 0.5$, and (e),(f) TW state for $c = 0.8$. Other parameters: $r_1 = 0.01$, $r_2 = 0.22$, $\epsilon = 2.7$, $\omega = 2.0$, $\lambda = 1.0$, and $N = 100$.

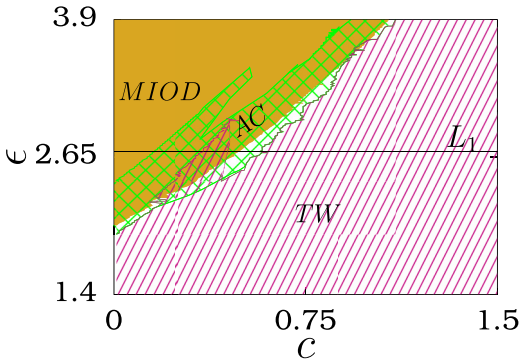

FIG. 14. Two-parameter bifurcation diagram in (c, ϵ) space. TW, AC, and MIOD represent the traveling wave, amplitude chimera, and multi-incoherent oscillation death state, respectively. Other parameter values are the same as in Fig. 1.

contrast with the earlier findings, in this case we found a reverse dynamical transition effect that is from an incoherent death state to a coherent traveling wave state via a stable amplitude chimera state as a function of the nonisochronicity parameter.

The global behavior with respect to the nonisochronicity parameter and the coupling strength is also illustrated in Fig. 14 in the (c, ϵ) parametric space. The traveling wave state is found to be stable in the entire range of c for lower values of ϵ, whereas there is a transition from a multi-incoherent death state to a traveling wave state via stable amplitude chimera as a function of c for higher values to ϵ. Multistability between the dynamical states is also observed in the boundary of TW-AC and AC-MIOD states.

We have also analyzed the transient nature of the dynamical states with respect to the nonisochronicity parameter (see Fig. 15) for the nonlocal coupling strength $\epsilon = 2.7$. The shaded region in Fig. 15(a) represents the stable amplitude

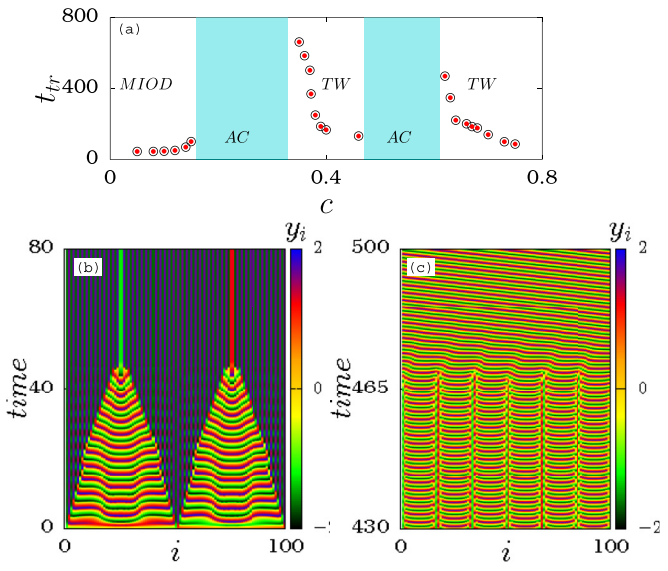

FIG. 15. (a) Transient time (t_{tr}) of distinct dynamical states as a function of nonisochronicity parameter c. Transient amplitude chimera at $\epsilon = 2.7$ for the nonisochronicity parameter, (a) $c = 0.1$ and (b) $c = 0.65$.

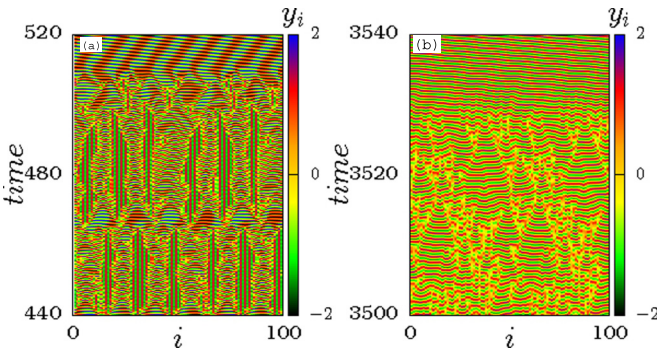

FIG. 16. Space-time plot for $\epsilon = 4.1$ for (a) $c = 1.0$, imperfect breathing chimera I and (b) $c = 2.5$, imperfect breathing chimera II. Other parameter values are the same as in Fig. 1.

chimera. The emergence of a stable MIOD state through transient AC is found for lower values of c, and the corresponding plot is shown in Fig. 15(b) for $c = 0.1$. At the MIOD region, the transient time increases with an increase in the nonisochronicity parameter, which is then stabilized to amplitude chimera at the critical value $c = 0.16$. Increasing the value of c further, destabilization of the amplitude chimera is observed and the system exhibits a stable traveling wave state through transient AC. In this region, the transient time decreases with an increase in the nonisochronicity parameter, and a sudden emergence of stable amplitude chimera is observed at $c = 0.47$, which is again destabilized by increasing c. Beyond $c = 0.62$, we found the existence of a stable TW state through transient AC [see Fig. 15(a)]. The transient AC observed in the traveling wave region at $c = 0.65$ is shown in Fig. 15(c), which clearly depicts that the oscillators in the coherent and incoherent domains merge to become a completely coherent domain resulting in the coherent traveling wave state.

In the earlier reports, the emergence of imperfect breathing chimera was reported for large values of the nonisochronicity parameters [39]. The system (1) also exhibits imperfect breathing chimera (see Fig. 16) as observed in the earlier reports but as transients. The imperfect breathing chimera states manifest as a traveling wave while increasing the transient time. The emergence of imperfect breathing chimera I and II as transient is evident from Figs. 16(a) and 16(b), which are stabilized to a traveling wave state upon increasing the transient time [39]. The nonisochronicity parameter is known

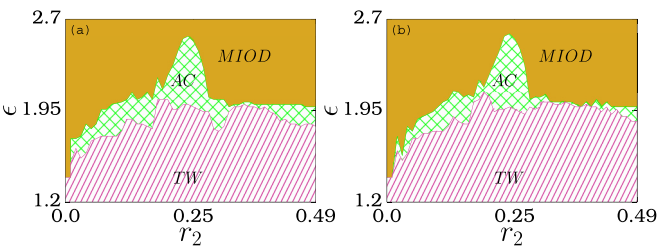

FIG. 17. Two-parameter bifurcation diagram in (r_2, ϵ) space for the noise intensity (a) $D = 0.001$ and (b) $D = 0.1$. TW, AC, and MIOD represent the traveling wave, amplitude chimera, and multi-incoherent oscillation death state, respectively. Other parameter values are the same as in Fig. 4.

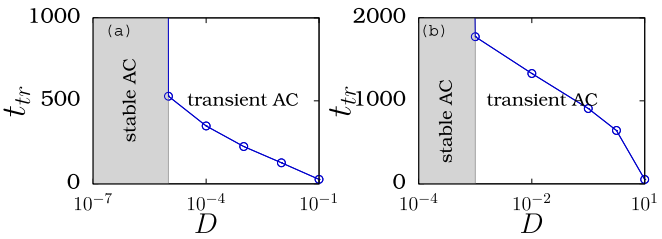

FIG. 18. Transient time of AC as a function of noise intensity D for (a) $r_2 = 0.16$ and $\epsilon = 1.8$, (b) $r_2 = 0.28$ and $\epsilon = 1.9$. Other parameters are the same as in Fig. 4.

to induce either a death state or a desynchronized state. In contrast, we found that it favors a traveling wave state from the death state via stable amplitude chimera.

The robustness of the stable amplitude chimera is also analyzed by introducing the Gaussian white noise into the system (1). Two-parameter bifurcation diagrams in (r_2, ϵ) space for the noise intensities $D = 0.001$ and 0.1 are depicted in Figs. 17(a) and 17(b), respectively. It is evident from the figures that traveling wave, amplitude chimera and MIOD states are intact in a large range of the parameter space even in the presence of a significant level of noise intensities thereby elucidating their robustness against noise.

Further, the transient time of the amplitude chimera is depicted as a function of the noise intensity D in Figs. 18(a) and 18(b) for two distinct repulsive coupling ranges and for the coupling strengths $\epsilon = 1.8$ and 1.9, respectively. The shaded region corresponds to the stable AC state, while the unshaded region corresponds to the transient AC state. It is evident from Figs. 18(a) and 18(b) that the stable amplitude chimera state loses its stability above the noise intensity 10^{-5} and 10^{-3} for the coupling ranges $r_2 = 0.16$ and 0.28, respectively, which then manifests as a traveling wave. It is also evident from the figure that the transient time ($t_{\rm tr}$) decreases upon increasing the noise intensity D [38]. Further, it is also observed that the amplitude chimera at the smaller and larger coupling ranges loses stability even at smaller noise intensities than the amplitude chimera in the midrange of r_2, where the spread of the amplitude chimera is large (see Fig. 4). Thus the amplitude chimera at the midrange of r_2 is more stable than the amplitude chimera at both extremes.

VIII. SUMMARY

In this work, we have investigated the emergence of stable amplitude chimera in a paradigmatic model of Stuart-Landau oscillators that are coupled nonlocally with combined attractive and repulsive couplings. The dynamical behavior of the considered system was analyzed for distinct initial conditions. We have reported the stabilization of amplitude chimera due to the presence of nonlocal repulsive coupling. In contrast with the earlier findings, the emergence of a stable amplitude chimera state was reported even for a random initial state while the stability of the corresponding dynamical state was also analyzed using the Floquet multipliers. Further, the transitions among the observed dynamical states were delineated by finding the average number of inhomogeneous oscillators. We have also reported that the transition among the dynamical states displays hysteresis behavior as a function of the coupling strength. The width of the hysteresis follows a bell-shaped function with a Gaussian fit as a function of the repulsive coupling range. The multistability regions were analyzed using the probability of states with respect to distinct initial states. We have also deduced the analytical stability curve that delineates the oscillatory (amplitude chimera and traveling wave) states from the death (multi-incoherent oscillation death, cluster chimera death, cluster oscillation death) states. Further, we have investigated the influence of the nonisochronicity parameter and noise intensity on the stable amplitude chimera. Increasing the nonisochronicity parameter favors the stabilization traveling wave from incoherent death via the stable amplitude chimera state. The stable AC loses its stability while increasing the noise intensity, and the transient time of AC decreases with an increase in the noise intensity.

ACKNOWLEDGMENTS

K.S. sincerely thanks the CSIR for fellowship under an SRF Scheme (09/1095(0037)/18-EMR-I). The work of V.K.C. forms part of a research project sponsored by INSA Young Scientist Project under Grant No. SP/YSP/96/2014 and SERB-DST Fast Track scheme for young scientists under Grant No. YSS/2014/000175. D.V.S. is supported by the CSIR EMR Grant No. 03(1400)/17/EMR-II. We acknowledge M. Lakshmanan for his encouragement and a critical reading of the manuscript.

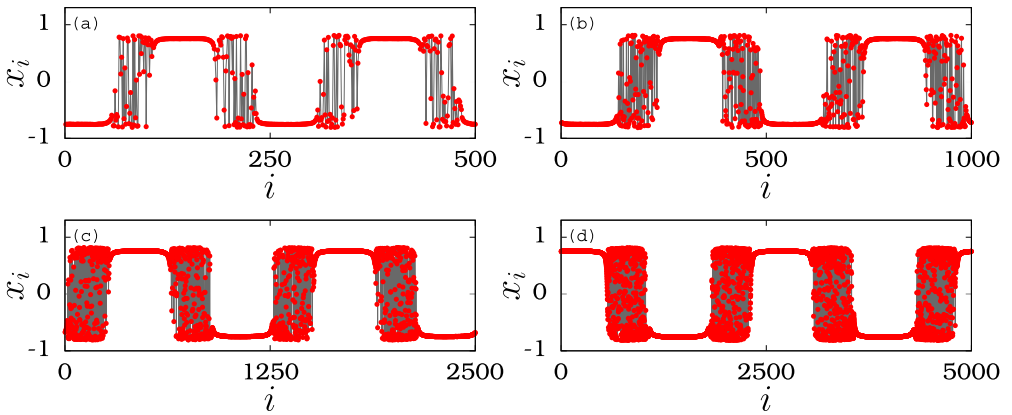

FIG. 19. Snapshots of stable amplitude chimera emerging from the network of different sizes for $\epsilon = 1.7$. (a) $N = 500$, (b) $N = 1000$, (c) $N = 2500$, and (d) $N = 5000$. Other parameters are the same as in Fig. 9.

APPENDIX: STABLE AC FOR DIFFERENT SIZES OF THE NETWORK

Snapshots of the variable x_i are depicted in Fig. 19 for different sizes N of the network to elucidate that the observed stable amplitude chimera state is independent of the size of the network. Further, even the structure of the amplitude chimera (two-cluster amplitude chimera) remains unaffected by the increase in the number of oscillators in the network, as is evident from Figs. 19(a)–19(d) for $N = 500$, 1000, 2500, and 5000, respectively.

[1] Y. Kuramoto and D. Battogtokh, Nonlinear Phenom. Complex Syst. **5**, 380 (2002).
[2] D. M. Abrams and S. H. Strogatz, Phys. Rev. Lett. **93**, 174102 (2004).
[3] S. I. Shima and Y. Kuramoto, Phys. Rev. E **69**, 036213 (2004).
[4] I. Omelchenko, B. Riemenschneider, P. Hövel, Y. Maistrenko, and E. Schöll, Phys. Rev. E **85**, 026212 (2012).
[5] N. I. Semenova, G. I. Strelkova, V. S. Anishchenko, and A. Zakharova, Chaos **27**, 061102 (2017).
[6] A. V. Cano and M. G. Cosenza, Phys. Rev. E **95**, 030202(R) (2017).
[7] J. Hizanidis, N. E. Kouvaris, G. Z. López, A. D. Guilera, and C. G. Antonopoulos, Sci. Rep. **6**, 19845 (2016).
[8] B. K. Bera, D. Ghosh, and M. Lakshmanan, Phys. Rev. E **93**, 012205 (2016).
[9] I. Omelchenko, Y. Maistrenko, P. Hövel, and E. Schöll, Phys. Rev. Lett. **106**, 234102 (2011).
[10] A. Bonsen, I. Omelchenk, A. Zakharova, and E. Schöll, Eur. Phys. J. B **91**, 65 (2018).
[11] C. R. Laing, Phys. Rev. E **81**, 066221 (2010).
[12] A. M. Hagerstrom, T. E. Murphy, R. Roy, P. Hövel, I. Omelchenko, and E. Schöll, Nat. Phys. **8**, 658 (2012).
[13] M. R. Tinsley, S. Nkomo, and K. Showalter, Nat. Phys. **8**, 662 (2012).
[14] E. A. Martens, S. Thutupalli, A. Fourriere, and O. Hallatschek, Proc. Natl. Acad. Sci. (U.S.A.) **110**, 10563 (2013).
[15] T. Kapitaniak, P. Kuzma, J. Wojewoda, K. Czolczynski, and Y. Maistrenko, Sci. Rep. **4**, 6379 (2014).
[16] L. V. Gambuzza, A. Buscarino, S. Chessari, L. Fortuna, R. Meucci, and M. Frasca, Phys. Rev. E **90**, 032905 (2014).
[17] L. Larger, B. Penkovsky, and Y. Maistrenko, Phys. Rev. Lett. **111**, 054103 (2013).
[18] M. Wickramasinghe and I. Z. Kiss, PLoS ONE **8**, e80586 (2013).
[19] L. Schmidt, K. Schönleber, K. Krischer and V. Garcia-Morales, Chaos **24**, 013102 (2014).
[20] M. Wickramasinghe and I. Z. Kiss, Phys. Chem. Chem. Phys. **16**, 18360 (2014).
[21] L. Larger, B. Penkovsky, and Y. Maistrenko, Nat. Commun. **6**, 7752 (2015).
[22] D. P. Rosin, D. Rontani, N. D. Haynes, E. Schöll, and D. J. Gauthier, Phys. Rev. E **90**, 030902(R) (2014).
[23] E. A. Viktorov, T. Habruseva, S. P. Hegarty, G. Huyet, and B. Kelleher, Phys. Rev. Lett. **112**, 224101 (2014).
[24] N. C. Rattenborg, C. J. Amlaner, and S. L. Lima, Neurosci. Biobehav. Rev. **24**, 817 (2000).
[25] N. C. Rattenborg, B. Voirin, S. M. Cruz, R. Tisdale, G. Dell'Omo, H. P. Lipp, M. Wikelski, and A. L. Vyssotski, Nat. Commun. **7**, 12468 (2016).
[26] M. Tamaki, J. W. Bang, T. Watanabe, and Y. Sasaki, Curr. Biol. **26**, 1190 (2016).
[27] A. Rothkegel and K. Lehnertz, New J. Phys. **16**, 055006 (2014).
[28] A. E. Motter, M. Gruiz, G. Károlyi, and T. Tél, Phys. Rev. Lett. **111**, 194101 (2013).
[29] J. C. Gonzalez-Avella, M. G. Cosenza, and M. S. Miguel, Physica A **399**, 24 (2014).
[30] C. R. Laing and C. C. Chow, Neural Comput. **13**, 1473 (2001).
[31] J. H. Sheeba, V. K. Chandrasekar, and M. Lakshmanan, Phys. Rev. E **81**, 046203 (2010).
[32] G. C. Sethia, A. Sen, and G. L. Johnston, Phys. Rev. E **88**, 042917 (2013).
[33] G. C. Sethia and A. Sen, Phys. Rev. Lett. **112**, 144101 (2014).
[34] B. W. Li and H. Dierckx, Phys. Rev. E **93**, 020202(R) (2016).
[35] A. Zakharova, M. Kapeller, and E. Schöll, Phys. Rev. Lett. **112**, 154101 (2014).
[36] L. Tumash, A. Zakharova, J. Lehnert, W. Just, and E. Schöll, Europhys. Lett. **117**, 20001 (2017).
[37] A. Gjurchinovski, E. Schöll, and A. Zakharova, Phys. Rev. E **95**, 042218 (2017).
[38] S. A. M. Loos, J. C. Claussen, E. Schöll, and A. Zakharova, Phys. Rev. E **93**, 012209 (2016).
[39] K. Premalatha, V. K. Chandrasekar, M. Senthilvelan, and M. Lakshmanan, Chaos **28**, 033110 (2018)
[40] G. Xiao, W. Liu, Y. Lan, and J. Xiao, Nonlin. Dyn. Springer **93**, 1047 (2018).
[41] K. Sathiyadevi, V. K. Chandrasekar, D. V. Senthilkumar, and M. Lakshmanan, Phys. Rev. E **97**, 032207 (2018).
[42] J. H. Sheeba, V. K. Chandrasekar, and M. Lakshmanan, Phys. Rev. Lett. **103**, 074101 (2009).
[43] K. Premalatha, V. K. Chandrasekar, M. Senthilvelan, and M. Lakshmanan, Phys. Rev. E **93**, 052213 (2016).
[44] A. Pikovsky, M. Rosenblum, and J. Kurths, *Synchronization: A Universal Concept in Nonlinear Sciences* (Cambridge University Press, New York, 2001).
[45] I. Schneider, M. Kapeller, S. Loos, A. Zakharova, B. Fiedler, and E. Schöll, Phys. Rev. E **92**, 052915 (2015).
[46] T. Aoyagi, Phys. Rev. Lett. **74**, 4075 (1995).
[47] N. Tukhlina and M. Rosenblum, J. Biol. Phys. **34**, 301 (2008).
[48] E. M. Izhikevich, *Dynamical Systems in Neuroscience: The Geometry of Excitability and Bursting* (MIT Press, Cambridge, MA, 2007).
[49] We have observed similar dynamical transitions even by switching the attractive and repulsive couplings among the variables. ϵ is the strength of the attractive and repulsive couplings.
[50] D. Yuan, F. Lin, L. Wang, D. Liu, J. Yang, and Y. Xiao, Sci. Rep. **7**, 42178 (2017).
[51] The best fit for the attractive coupling range $r_1 = 0.2$ is $(a, b) = (1, -0.613)$ and the best fit for $r_1 = 0.4$ is $(a, b) = (1, -0.569)$.